APSB
Acta Pharmaceutica Sinica B
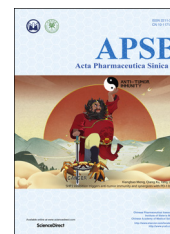
ORIGINAL ARTICLE

Cytotoxic and antibacterial polyketide-indole hybrids synthesized from indole-3-carbinol by *Daldinia eschscholzii*

Liping Lin[a,b], Nan Jiang[c], Huimin Wu[b], Yaning Mei[d], Jie Yang[e], Renxiang Tan[a,b,*]

[a]State Key Laboratory Cultivation Base for TCM Quality and Efficacy, Nanjing University of Chinese Medicine, Nanjing 210046, China
[b]State Key Laboratory of Pharmaceutical Biotechnology, Nanjing University, Nanjing 210023 China
[c]School of Pharmacy, Nanjing Medical University, Nanjing 210029, China
[d]Department of Clinical Laboratory, the First Affiliated Hospital of Nanjing Medical University, Nanjing 210029, China
[e]Jiangsu Province Academy of Traditional Chinese Medicine, Nanjing 210028, China

Abstract Two skeletally undescribed polyketide-indole hybrids (PIHs), named indolchromins A and B, were generated from indole-3-carbinol (I3C) in the fungal culture (*Daldinia eschscholzii*). The indolchromin structures were elucidated mainly by their 1D and 2D NMR spectra with the former confirmed by the single-crystal X-ray crystallographic analysis. Each indolchromin alkaloid was chirally separated into four isomers, whose absolute configurations were assigned by comparing the recorded circular dichroism (CD) spectra with the electronic CD (ECD) curves computed for all optional stereoisomers. Furthermore, the indolchromin construction pathways in fungal culture were clarified through enzyme inhibition, precursor feeding experiment, and energy calculation. The cascade reactions, including decarboxylative Claisen condensation catalyzed by 8-amino-7-oxononanoate synthase (AONS), $C(sp^3)$-H activation, double bond migration, and Michael addition, all undergone compatibly during the fungal cultivation. In an MIC range of 1.3–8.6 μmol/L, (2*S*,4*R*)- and (2*R*,4*S*)-indolchromin A and (2*R*,4*S*)-indolchromin B are inhibitory against *Clostridium perfringens*, *Clostridium difficile*, *Veillonella* sp., *Bacteroides fragilis*, and *Streptococcus pyogenes*. (2*R*,4*S*)-Indolchromin A and (2*S*,4*S*)-indolchromin B were cytotoxic against the human breast cancer cell line MDA-MB-231 with IC_{50} values of 27.9 and 131.2 nmol/L, respectively, with the former additionally active against another human breast cancer cell line MCF-7 (IC_{50} 94.4 nmol/L).

*Corresponding author at: State Key Laboratory Cultivation Base for TCM Quality and Efficacy, Nanjing University of Chinese Medicine, Nanjing 210023, China.
 E-mail address: rxtan@nju.edu.cn (Renxiang Tan).

1. Introduction

Indole alkaloids are an important class of organic molecules that contain one or more indole or indoline motifs. They widely distribute as secondary metabolites in bacteria, fungi, plants and animals[1–3]. Some indole alkaloids have been demonstrated to be cytotoxic (*e.g.*, vintafolide and lestaurtinib[4]), analgesic (*e.g.*, physostigmine[5]), antibacterial (*e.g.*, dalesindole[6]), neuritogenic (*e.g.*, manzamines[7]), immunosuppressive (*e.g.*, sotrastaurin and tivantinib[4]), stem cell differentiation regulatory (*e.g.*, kenpaullone and stauprimide[8]), and others. Therefore, the indole motif is present in diverse pharmacophores and many research groups have been motivated to discover more bioactive new alkaloids branded with such motifs[9–11].

Polyketides are among the most diverse natural product categories[12], but few polyketide-indole hybrids (PIHs) have been synthesized chemically or characterized from nature except for the tryptophan-derived cytochalasans[3]. A presumable underlying reason for the PIH rarity arises from the fact that the PIH synthesis faces a suite of challenges, such as the complicated reaction steps (including iterative/inevitable procedures for protection and deprotection) and/or the utilization of toxic/expensive reagents[13,14]. Strategically, the generation of new PIHs usually includes cascade reactions such as C–C(N/O) bond formation[15] and selective functionalization of unactivated aliphatic C(sp^3)–H bonds[16]. However, these reactions largely proceed in harsh reaction conditions[17]. Thus, the greener approach is highly desired for the access to undescribed PIH molecules, and preferably, the PIH-constructing reactions could be completed in one pot in an eco-friendly manner.

Indole-3-carbinol (I3C, **1**) is a cancer-preventive agent[18] released *via* the degradation of indole glucosinolate in cruciferous vegetables[19,20]. After its oral administration to mice, **1** is metabolized into indole alkaloids including indole-3-carbaldehyde (I3A), indole-3-carboxylic acid (I3CA, **2**), 1-(3-hydroxymethyl)-indolyl-3-
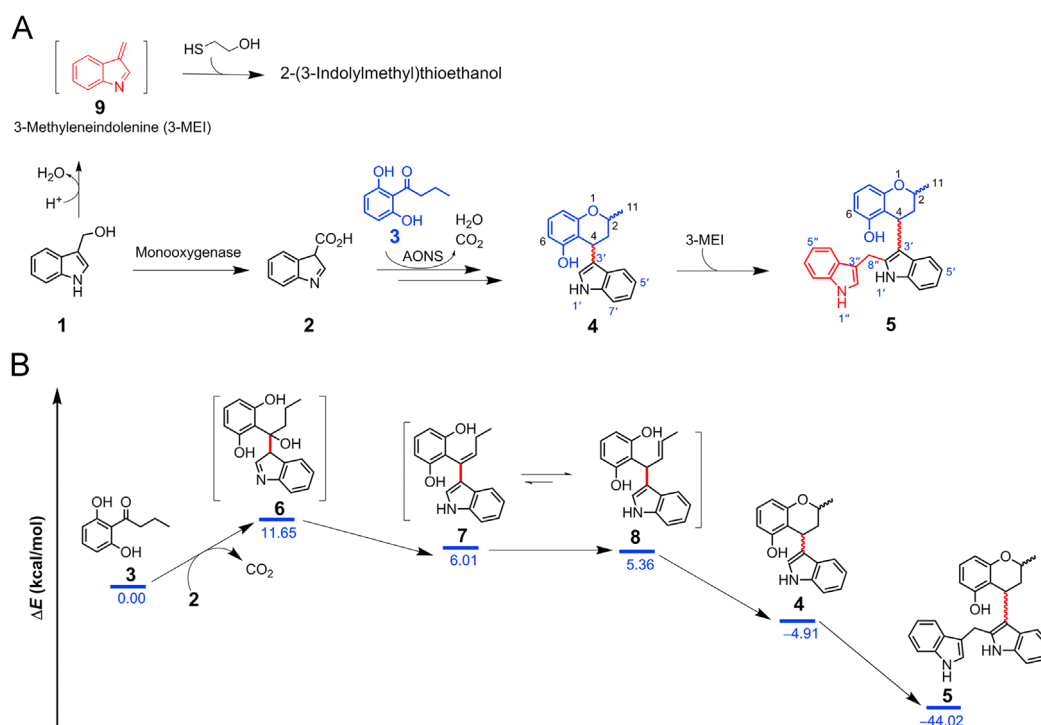
Scheme 1 Indolchromins A (**4**) and B (**5**) resulting from the coupling of fungal polyketide with I3C (**1**) catabolites. (A) Proposed polyketide-indole hybridization leading to **4** and **5** in the I3C exposed fungal culture. (B) Reaction energy profile for the generation of **4** and **5** computed by DFT method at B3LYP/6-31+G(d,p) level in polarizable continuum model (PCM, dielectric constant $\varepsilon = 78.39$ for H_2O). The relative energies in kcal/mol are calculated from the sums of the respective total energies (E_{sol}) of all species (Supporting Information Table S2). AONS, 8-amino-7-oxononanoate synthase; I3CA (**2**), indole-3-carboxylic acid.

indolylmethane (HI-IM), 3,3′-diindolylmethane (DIM), indolo[3,2*b*] carbazole (ICZ), and 2-(indol-3-ylmethyl)-3,3′-diindolylmethane (LTr1)[21]. The tumor therapeutic effect of DIM as a drug candidate under the phase III clinical trial (http://www.clinicaltrials.gov) could be alternatively formed by the decarboxylative Claisen condensation between I3A and I3CA (2), which was catalysed by 8-amino-7-oxononanoate synthase (AONS) in *Daldinia eschscholzii*[6]. Encouraged by the observation, we wondered whether 1 could be further metabolized and hybridized with polyketides, such as 1-(2,6-dihydroxyphenyl)-butan-1-one (3) from *D. eschscholzii*[22,23], to afford new PIHs. The ketone and/or ketone-activated methylene might be able to form C–C (N/O) bonds with I3C-derived metabolites such as 2, I3A, and 3-methyleneindolenine (3-MEI)[24]. Herein, we present that the fungal polyketide reacts with the I3C metabolites most likely under the AONS catalysis to initialize the formation of indolchromins A (4) and B (5) (Scheme 1), two skeletally undescribed PIHs with potent antibacterial and cytotoxic activities.

2. Results and discussion

The work began with the regrowth of *D. eschscholzii* in exposure to I3C (1). The extract derived from the fungal culture was chromatographed to afford an alkaloid-containing fraction, which was separated into subfractions I and II. As detailed in Section 4.7.1, the first alkaloid was isolated from subfraction I as yellow crystals and named indolchromin A (4) after the I3C-originated indole and polyketide-derived chromane moieties. The molecular formula of 4 was evidenced to be $C_{18}H_{17}NO_2$ from the Na^+-liganded molecular ion at *m/z* 302.1156 ($C_{18}H_{17}NO_2Na$ requires 302.1152) in its high-resolution electrospray ionization mass spectrometry (HR-ESI-MS). The ^1H NMR spectrum of 4 displayed the signals arising from one 3-substituted indole (C-2′–C-7′a) and a 4-substituted 2-methylchromane (C-2∼C-11) scaffolds (Supporting Information Fig. S3). This observation, along with the C-3′/4 linkage, was reinforced by the 2D NMR spectra of 4 (Fig. 1 and Supporting Information Figs. S6–S8), which allowed unambiguous assignments of its ^1H and ^{13}C NMR data (Table 1 and Supporting Information Figs. S3–S5). The relative configuration of C-2 and C-4 was deduced from the magnitude of coupling constants $J_{2,3a}$ (1.8 Hz), $J_{2,3b}$ (12.4 Hz), $J_{3a,4}$ (1.8 Hz), and $J_{3b,4}$ (5.2 Hz), which accommodated the *trans*-oriented H-2 and H-4[25] (Fig. 2 and Table 1). This was substantiated by its NOESY spectrum displaying the expected correlation of H-4 with H-11 (the methyl proton) (Supporting Information Fig. S9), and by the NOE enhancement of the H-11 doublet discerned upon irradiating the H-4 resonance (Supporting Information Fig. S10). This relative configuraion was further confirmed by its single-crystal X-ray (Fig. 1) crystallographic analysis detailed in Section 4.6.

However, the space group P21/c of crystal 4 indicted its racemate nature. Subsequent chiral HPLC separation of 4 afforded two enantiomers (Supporting Information Fig. S1) which were clarified to be (2*S*,4*R*)-4 and (2*R*,4*S*)-4 (Fig. 2A) by comparing their circular dichroism (CD) spectra with the electronic CD (ECD) curves calculated for all of its optional stereoisomers using quantum mechanical time-dependent density functional theory (TD-DFT, Fig. 2A). In theory, a two-chiral-carbon molecule should have four stereoisomers, suggesting the possible presence of two more enantiomers of 4. Therefore, the mother liquors derived from subfraction I were combined and refractionated to give a crystal (4′), which was identical to 4 in molecular weight and formula with its ^1H and ^{13}C NMR spectra similar to those of (2*S*,4*R*)-4 and (2*R*,4*S*)-4 (Figs. 1 and 2B and Table 1). However, the *cis*-oriented H-2 and H-4 were determined by the coupling constants $J_{2,3a}$ (2.0 Hz), $J_{2,3b}$ (14.0 Hz), $J_{3a,4}$ (7.6 Hz), and $J_{3b,4}$ (10.5 Hz)[25] (Fig. 2B and Table 1) and confirmed by its single-crystal X-ray crystallographic analysis (Fig. 1). This observation agreed with the absence of the NOESY correlation between H-4 and H-11 (Supporting Information Fig. S13). Similarly, the X-ray diffraction of 4′ (Fig. 1) underpinned its racemate nature with space group P21 21 21, which was detailed in Section 4.6. Subsequent chiral HPLC resolution of 4′ supplied a pair of enantiomers (Supporting Information Fig. S2) with identical ^1H and ^{13}C NMR spectra (Fig. 2B and Table 1) but reverse CD curves (Fig. 2A). The absolute configuration of the two enantiomers was assigned to be (2*S*,4*S*)-4 and (2*R*,4*R*)-4 by the comparing the recorded CD curves (black solid line) with the ECD spectra (red dash line) computed for all optional stereoisomers of 4 (Fig. 2A).

According to our previous endeavor[6], 4 might be prone to Michael addition reaction, too. This rationalization encouraged us to fractionate another alkaloid-containing portion, subfraction II, to give a brown powder which was named indolchromin B (5, Section 4.7.1). Compound 5 exhibited a Na^+-liganded molecular ion at *m/z* 431.1731 in its HR-ESI-MS ($C_{27}H_{24}N_2O_2Na$ requires 431.1730). In the ^1H NMR spectrum of 5 (Table 1, Fig. 3 and Supporting Information Fig. S16), the presence of 3-indolylmethyl and 5-hydroxychromane units was determined by comparing with those of 4. However, the existence of an additional 3-indolylmethyl was indicated by a group of typical proton signals at δ 10.05 (br s), 6.76 (dd, J = 5.2, 2.0 Hz), 6.76 (t, J = 8.0 Hz), 6.89 (t, J = 8.0 Hz), 7.16 (d, J = 8.0 Hz), and 4.13 (br s). This 3-indolylmethyl group was demonstrated to anchor on C-2′ which resonated at $δ_C$ 135.7, being moved downfield by 9.4 ppm from that ($δ_C$ 126.3) of 4. The *trans*-oriented H-2 and H-4 of 5 were deduced from the coupling constants $J_{2,3a}$ (2.0 Hz), $J_{2,3b}$ (12.4 Hz), $J_{3a,4}$ (2.0 Hz), and $J_{3b,4}$ (5.2 Hz)[25] (Fig. 3 and Table 1),
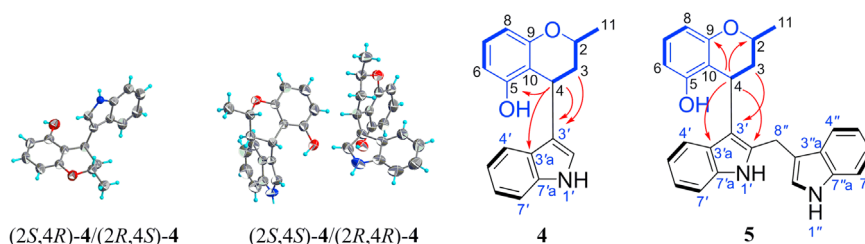

Figure 1 Structures of indolchromins A (4) and B (5). Racemate crystal structures of (2*S*,4*R*)-4/(2*R*,4*S*)-4 and (2*S*,4*S*)-4/(2*R*,4*R*)-4. Planar structures of 4 and 5 (HMBC, red arrows (H→C); ^1H–^1H COSY, bold lines).

Table 1 ^{1}H (400 MHz) and ^{13}C NMR (100 MHz) data for **4** and **5** (δ in ppm, J in Hz, acetone-d_6)[a,b].

Position	(2S,4R)-4 and (2R,4S)-4		(2R,4R)-4 and (2S,4S)-4		(2S,4R)-5 and (2R,4S)-5		(2R,4R)-5 and (2S,4S)-5	
	δ_C	δ_H	δ_C	δ_H	δ_C	δ_H	δ_C	δ_H
2	67.5	4.07 (dqd, 12.4, 6.4, 1.8)	68.4	4.08 (dqd, 14.0, 6.4, 2.0)	69.4	4.30 (dqd, 12.4, 6.4, 2.0)	72.0	4.17 (br qd, 12.8, 6.4)
3α	35.5	2.18 (dt, 13.4, 1.8, H-3α)	35.1	2.40 (ddd, 14.0, 7.6, 2.0, H-3α)	38.9	2.00 (dt, 13.2, 2.0)	38.6	2.26 (m)
3β		1.90 (ddd, 13.4, 12.4, 5.2, H-3β)		2.00 (td, 14.0, 10.5, H-3β)		1.96 (ddd, 13.2, 12.4, 5.2)		2.01 (m)
4	27.4	4.63 (dd, 5.2, 1.8)	28.2	4.56 (dd, 10.5, 7.6)	28.5	4.76 (dd, 5.2, 2.0)	29.1	4.69 (dd, 11.2, 8.0)
5	155.8		155.1		157.6		156.9	
5-OH		7.89 (s)		7.25 (s)		7.83 (s)		
6	107.8	6.41 (dd, 8.0, 1.2)	108.3	6.44 (dd, 8.0, 1.2)	107.4	6.38 (d, 8.0)	108.4	6.23 (dd, 8.0, 0.8)
7	127.3	6.98 (t, 8.0)	126.9	6.96 (t, 8.0)	128.8	6.98 (t, 8.0)	127.2	6.97 (t, 8.0)
8	106.6	6.39 (dd, 8.0, 1.2)	105.9	6.25 (dd, 8.0, 1.2)	108.7	6.42 (d, 8.0)	107.9	6.43 (dd, 8.0, 0.8)
9	156.5		156.4		157.1		157.1	
10	111.4		110.9		113.1		112.3	
11	20.8	1.26 (d, 6.4)	20.2	1.35 (d, 6.4)	21.8	1.27 (d, 6.4)	20.7	1.32 (d, 6.4)
1′		9.89 (br s)		10.11 (br s)		9.56 (br s)		9.84 (br s)
2′	123.5	6.59 (d, 2.4, 0.8)	123.5	6.67 (br s)	135.7		135.6	
3′	119.8		118.9		114.7		112.7	
3′a	126.3		126.3		129.6		126.8	
4′	118.6	7.65 (br d, 8.0)	117.5	7.40 (br d, 8.0)	119.5	7.48 (d, 8.0)	118.4	7.56 (br s)
5′	118.5	7.02 (td, 8.0, 0.8)	117.8	6.90 (td, 8.0, 0.8)	119.4	6.91 (t, 8.0)	118.6	6.94 (t, 8.0)
6′	121.2	7.11 (td, 8.0, 0.8)	120.8	7.09 (td, 8.0, 0.8)	122.2	7.06 (t, 8.0)	120.5	6.93 (t, 8.0)
7′	111.4	7.39 (br d, 8.0)	110.9	7.26 (br d, 8.0)	112.0	7.37 (d, 8.0)	110.8	7.22 (d, 8.0)
7′a	137.3		137.3		136.6		135.6	
1″						10.05 (br s)		10.09 (br s)
2″					124.5	7.17 (s)	123.5	7.21 (s)
3″					112.6		112.6	
3″a					128.4		127.4	
4″					119.8	6.76 (d, 8.0)	119.8	6.59 (br s)
5″					119.1	6.76 (t, 8.0)	118.4	6.76 (br s)
6″					120.8	6.89 (t, 8.0)	121.4	7.12 (t, 8.0)
7″					111.4	7.16 (d, 8.0)	112.9	7.38 (d, 8.0)
7″a					137.8		136.9	
8″					22.8	4.13 (br s)	22.1	4.40 (br s)

[a]Assigned by the ^{1}H–^{1}H COSY, HSQC, and HMBC spectra.
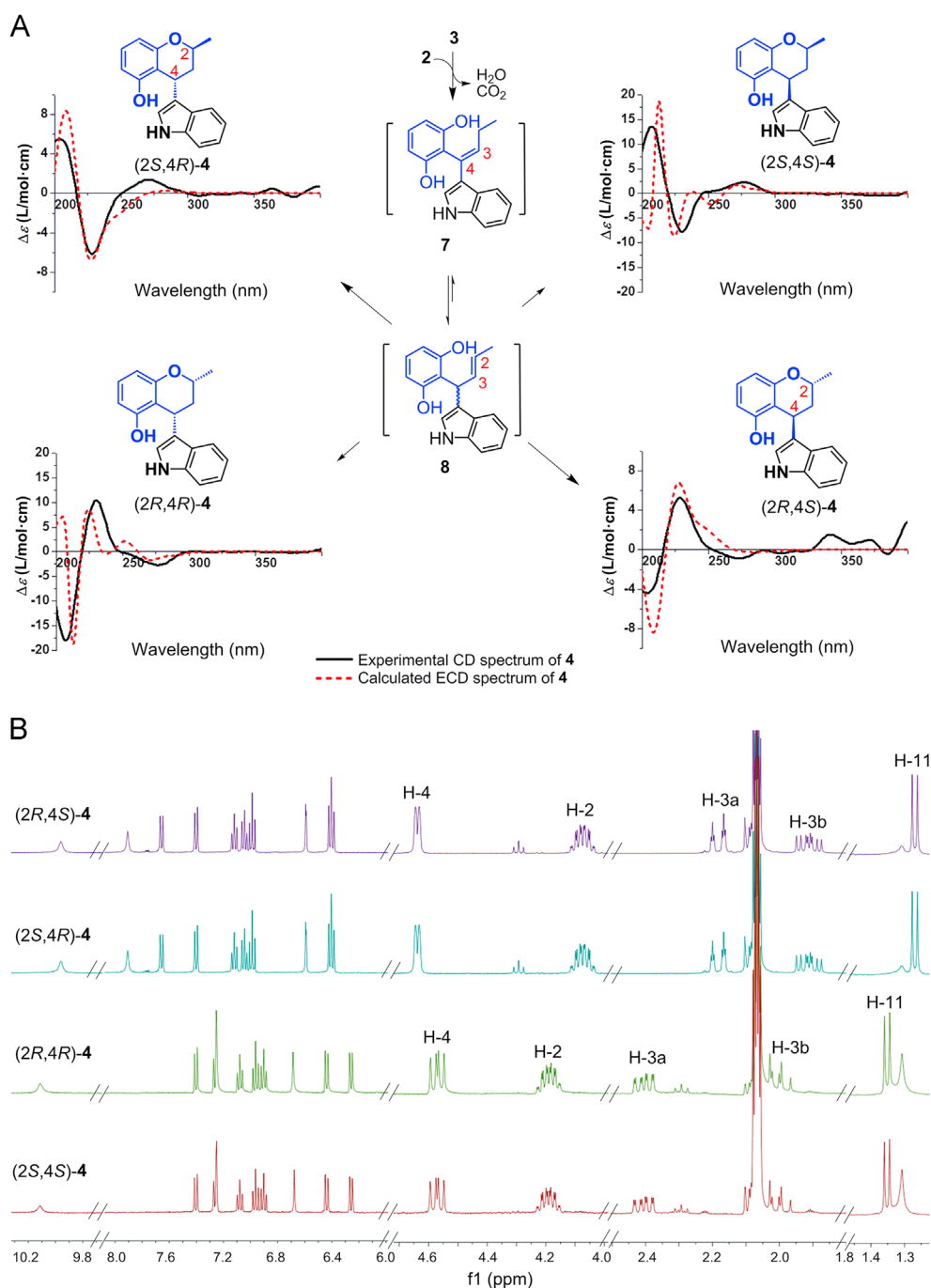[b]Enantiomers in a racemate have identical ^{1}H and ^{13}C NMR data.

Figure 2 Stereoisomers for indolchromin A (**4**). (A) Stereochemical assignment for the major [(2*S*,4*R*)-**4** and (2*R*,4*S*)-**4**] and minor [(2*R*,4*R*)-**4** and (2*S*,4*S*)-**4**] enantiomer pairs by comparing each recorded CD spectrum with those computed for all options. (B) The difference between the ¹H NMR spectra of major and minor stereoisomer pairs.

which accorded with the NOESY correlation between H-4 and H-11 (Supporting Information Fig. S22). It is noteworthy that this set of coupling constants is almost identical to the counterpart of (2*S*,4*R*)-**4** and (2*R*,4*S*)-**4** (Table 1). Chiral HPLC separation of **5** (Supporting Information Fig. S14) afforded (2*S*,4*R*)-**5** and (2*R*,4*S*)-**5**, which have identical ¹H and ¹³C NMR spectra (Table 1 and Fig. 3B) but reverse CD curves (Fig. 3A). Their absolute configuration was established by comparing the recorded CD curves (black line) with the ECD spectra (red line) computed for all optional stereoisomers (Fig. 3A).

Inspired by the discovery of (2*S*,4*S*)-**4** and (2*R*,4*R*)-**4**, the mother liquors derived from subfraction II were combined and refractionated to give powder **5′**, which was identical to **5** in molecular weight and formula. However, **5′** was slightly different from **5** in the ¹H and ¹³C NMR spectra indicating that **5′** was most likely an isomer of **5** (Table 1, Fig. 3, and Supporting Information Fig. S23). In the ¹H NMR spectra of **5′**, the signals of H-3, H-4′, and H-4″ were broadened by their long-range couplings with H-11, H-7′, and H-7″ (Fig. 3B and Supporting Information Figs. S26–S27), respectively, as encountered elsewhere[26,27]. But this did not create any difficulty
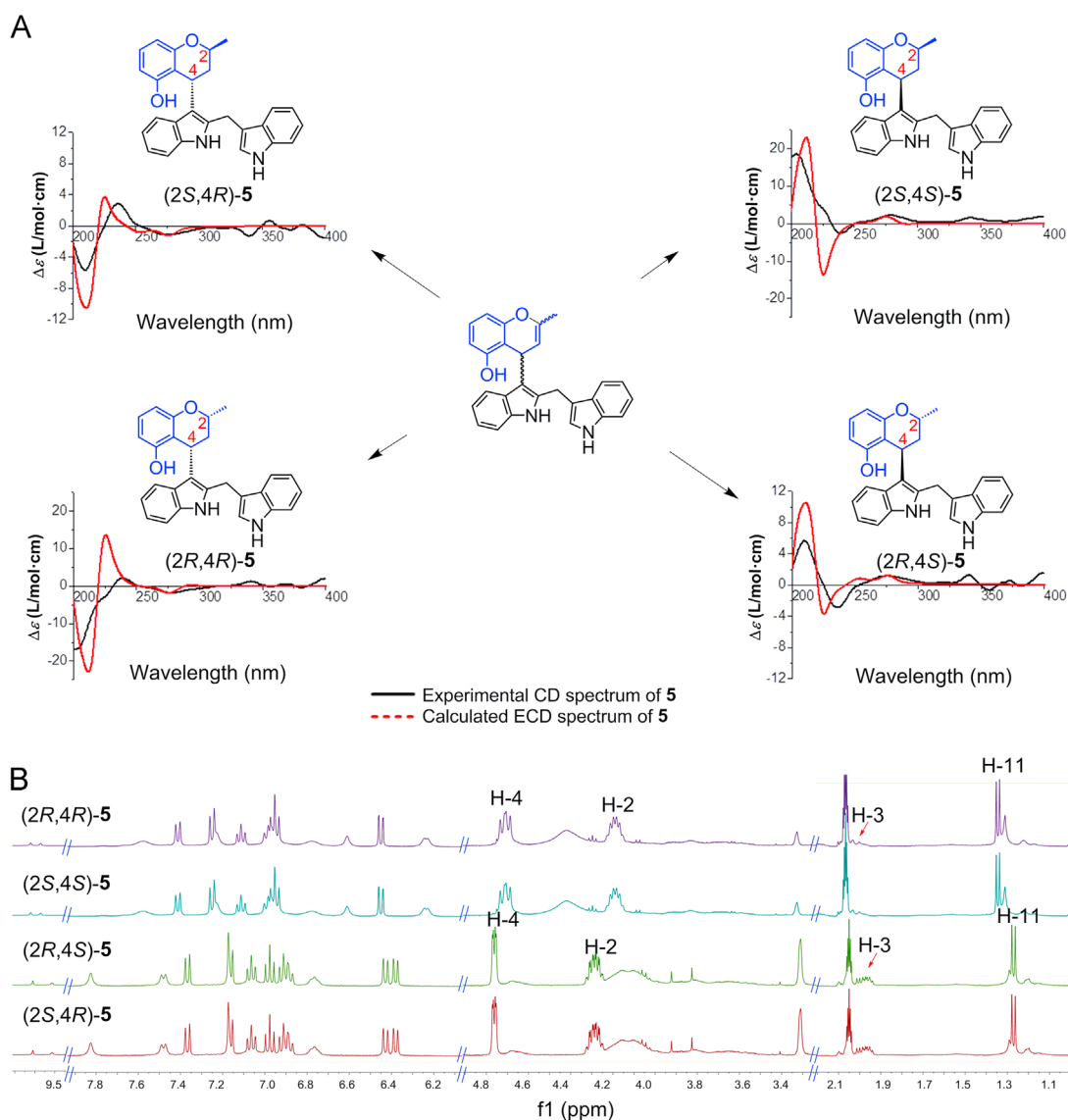
Figure 3 Stereoisomers of indolchromin B (**5**). (A) Stereochemical assignment for the major [(2S,4R)-**5** and (2R,4S)-**5**] and minor [(2R,4R)-**5** and (2S,4S)-**5**] enantiomer pairs by comparing each recorded CD spectrum with those computed for all options. (B) The difference between the ¹H NMR spectra of major and minor stereoisomer pairs.

Table 2 Antibacterial activity of 4 and 5 (MICs in μmol/L).

Compd.	Cp	Cd	*Veillonella* sp.	Bf	Bs	Sa	Sp	Xoo	Ea
(2S,4R)-**4**	2.5	2.5	5.0	6.4	>10	>10	2.1	>10	>10
(2R,4S)-**4**	1.3	2.5	5.0	6.2	>10	>10	5.0	>10	>10
(2S,4S)-**5**	>10	>10	>10	>10	>10	7.2	8.6	>10	>10
(2R,4S)-**5**	6.7	6.3	>10	>10	>10	>10	7.2	>10	>10
Streptomycin	ND	ND	ND	ND	7.5	0.5	4.0	0.9	1.1
Tinidazole	1.01	2.02	1.01	4.04	ND	ND	4.04	ND	ND

Bf, *Bacteroides fragilis*; Bs, *Bacillus subtilis*; Cp, *C. perfringens*; Cd, *C. difficile*; Ea, *Erwinia amylovory*; Sa, *Staphylococcus aureus*; Sp, *Streptococcus pyogenes*; Xoo, *Xanthomonas oryzae* pv. *oryzicola*. ND = not detected.

in retrieving the coupling constants of H-3a and H-3b with H-2 and H-4, which resonated as clearly split signals at δ 4.17 (dq, J = 12.8, 6.4 Hz) and 4.69 (dd, J = 11.2, 8.0 Hz) (Table 1 and Supporting Information Fig. S23), respectively. Accordingly, the *cis*-

oriented H-2 and H-4 of **5**′ were convincingly defined by the typical coupling constants ($J_{2,3b}$, 12.8 Hz; $J_{3a,4}$, 8.0 Hz; and $J_{3b,4}$, 11.2 Hz), the absence of the NOESY correlation between H-4 and H-11 (Table 1 and Supporting Information Fig. S30)[25], and the
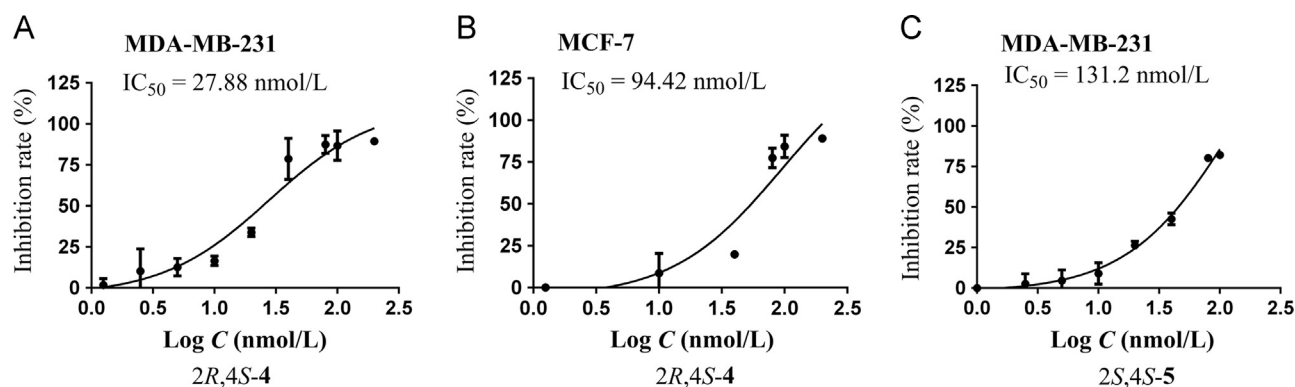
Figure 4 Cytotoxic stereoisomers of **4** and **5**.

Table 3 Cytotoxicity of (2S,4R)-4 and (2S,4S)-5 (IC_{50} in μmol/L).

Compd.	SW480	HL-60	HepG-2	A375	MCF-7	CaoV-3	A549	MDA-MB-231
(2R,4S)-**4**	13.61 ± 0.85	12.10 ± 1.22	14.07 ± 0.97	>15	0.09442	13.59 ± 1.10	>15	0.02788 ± 0.95
(2S,4S)-**5**	13.49 ± 1.34	11.24 ± 0.55	13.59 ± 1.42	14.10 ± 1.16	>15	9.51 ± 0.53	>15	0.1312 ± 1.37
Doxorubicin	1.17 ± 0.11	0.87 ± 0.04	2.60 ± 0.18	1.95 ± 0.09	8.71 ± 0.15	2.04 ± 0.37	1.76 ± 0.13	8.00 ± 0.02

indiscernibility of the H-4 NOE enhancement upon irradiating the H-11 signal (Supporting Information Fig. S31). Similarly, C-2′ was demonstrated to carry a 3-indolylmethyl group by its HMBC correlation with H-4 (δ_H 4.69) and by the downfield C-2′ from δ_C 123.5 to 135.6 (Fig. 1 and Table 1). Chiral HPLC separation of **5′** afforded (2R,4R)-**5** and (2S,4S)-**5** (Supporting Information Fig. S15), which were stereochemically assigned by comparing their CD spectra with the ECD curves calculated for all possible stereoisomers of **5** (Fig. 3A).

With all stereoisomers of **4** and **5** in hand, we were motivated to evaluate their biological property. In view of pathogenic threat to human health and crop production[28–30], the *in vitro* antibacterial assay[31] was prioritized as the first evaluation window. In an MIC range of MICs, 1.3–8.6 μmol/L, (2S,4R)-**4** and (2R,4S)-**4** were shown to be inhibitory on the growth of four anaerobic (*Clostridium perfringens*, *C lostridium difficile*, *Veillonella* sp., and *Bacteroides fragilis*) and a Gram-positive bacteria (*Streptococcus pyogenes*) (Table 2). (2S,4R)-**5** exhibited potent antibacterial activities on *C. perfringens*, *C. difficile* and *S. pyogenes* but not on *Veillonella* sp., while (2S,4S)-**5** was only shown to effect on the growth of *S. aureus* and *S. pyogenes*. The observed potency was comparable to those of co-assayed streptomycin and tinidazole (Table 2). Furthermore, all stereoisomers of **4** and **5** were assessed for the cytotoxic activity as outlined elsewhere[32]. As a result, (2S,4R)-**4** and (2S,4S)-**5** were inhibitories against the human breast cancer cell line MDA-MB-231 with IC_{50} values of 27.9 and 131.2 nmol/L, respectively. Moreover, (2S,4R)-**4** is also active against another human breast cancer cell line MCF-7 (IC_{50}: 94.4 nmol/L) (Fig. 4). However, doxorubicin, an anticancer drug, was co-assayed with the IC_{50} values being 8.0 and 8.7 μmol/L against the MDA-MB-231 and MCF-7 cell lines, respectively (Table 3).

Since the biological activity of **4** and **5** is chirality-dependent, we were obligated to address the generation process towards these stereoisomers. Inspired by the oxidation of I3C (**1**) into I3CA (**2**)[6], the formation of **4** could be triggered by the decarboxylative Claisen condensation between **2** and **3** *via* a newly formed C_4–C_3 bond (Scheme 1). Such a Claisen-condensing process was calculated to be energetically unfavorable[33,34] (Scheme 1B) and found to be catalysed by AONS since **4** disappeared upon the fungal exposure to the AONS inhibitors-D-cycloserine, plumbagin, and triphenyltin acetate (Fig. 5A) as described in Section 4.9.1. The ensuing cascade reactions including the dehydration, double bond migration resulted in $C(sp^3)$-H activation, and intramolecular cyclization might occur to give **4** (Scheme 1B), which was computed to be energetically favourable and non-enzymatic (Scheme 1B), thereby allowing the generation of all the four possible stereoisomers. In particular, the transformation of intermediate **6** into **4** *via* transient molecules **7** and **8** may be allowed by the poor or negligible conjugation of the double bond with the two sterically hindered aromatic substituents and propelled by the steric hindrance release *via* the chromane ring formation. Thus, the stereoisomers of **4** and **5** were ascertained to be hardly interchangeable (Scheme 1), and this differs from the dalesindole's isomerization[6]. To confirm this assumption, each stereoisomer of **4** and **5** was exposed to fungal proteins or in the phosphate buffer. As a result, they all stood stable within 48 h. Furthermore, the proposed conversion of **4** into **5** was calculated to be energetically favorable, which was demonstrated to be non-enzymatic by the formation of **5** upon stirring **4** in phosphate buffer with exposure to air and I3C (**1**, as precursor of 3-MEI) (Fig. 5B, Scheme 1, and Section 4.9.2). Though impossible to verify experimentally, the compounding of **2** with **3** into **4**, and eventually to **5** after incorporating 3-MEI, was computed to be quite feasible (Scheme 1B).

Since 5-hydroxy-2-methylchroman-4-one forms readily from **3** *via* an intramolecular cyclization[6], we wondered whether this chromanone could be also the precursor for generating **4** and **5**. To clarify the ambiguity, the chromanone and **3** were individually exposed, in the presence of I3C (**1**), to the intracellular fungal protein (IFP) pre-permeated against dialysis bag (MD 31) to remove all small molecules (Section 4.9.3). As a result, **4** and **5** were generated through the IFP catalyzed reaction of **1** with **3**, but not 5-hydroxy-2-methylchroman-4-one (Scheme 1 and Fig. 6A). These experiments confirmed the involvement of **3** in the
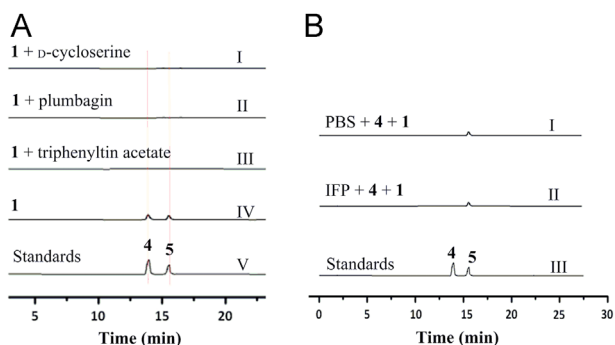
Figure 5 Construction pathways of indolchromins A (**4**) and B (**5**). (A) AONS is involved in the indolchromin production since **4** and **5** became undetectable if the I3C supplemented fungal culture was exposed additionally to any of the AONS inhibitors D-cycloserine (I), plumbagin (II) and triphenyltin acetate (III) at 1.0 mmol/L. (B) Non-enzymatic formation of **5** from **4** *via* incorporating 3-MEI [freshly derived from I3C (**1**), see Scheme 1].
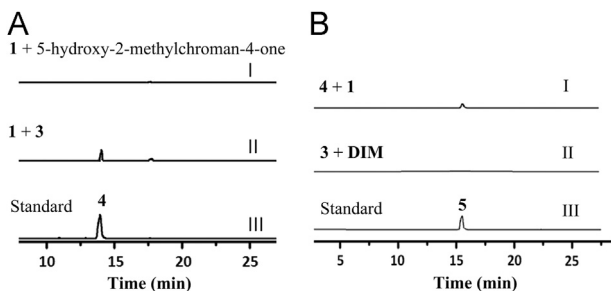

Figure 6 Identification of the precursor of indolchromins A (**4**) and B (**5**). (A) Compound **4** was formed by co-exposing **1** and **3** to the intracellular fungal protein (IFP), but failed to be detected if IFP was mixed with **1** and 5-hydroxy-2-methylchroman-4-one. (B) Compound **5** was generated when exposing IFP to **4** and **1** (as a 3-MEI precursor), but not produced if IFP was mingled with to **3** and DIM.

formation of **4** and **5**. Furthermore, I3C (**1**) may dehydrate to form 3-MEI in parallel with its oxidation into **2**. This was confirmed by the capture of 3-MEI by 2-mercaptoethanol in the work (Scheme 1, Supporting Information Scheme S1 and Fig. S32). Recognizing 3-MEI as an active intermediate, **5** could be generated either by the coupling of **4** with 3-MEI or by the condensation of **3** with I3C-derived 3,3′-diindolylmethane (DIM)[6] as specified in Section 4.9.4. However, co-exposure of **3** and DIM to IFP failed to form **5**, thereby discarding the latter option (Fig. 6B).

3. Conclusions

Many indoles and polyketides are reported, but polyketide-indole hybrids (PIHs) remain quite rare. In this study, eight new PIH isomers were isolated and characterized from the I3C-exposed culture of *D. eschscholzii*. Distinct from the chemical synthesis of indolyl polyketides[35], these PIHs feature a carbon–carbon bond formation of the indolyl C-3 with the chromone ketone in one pot without adding catalyst. The relative configurations of all

stereoisomers were assigned by couple constants, NOESY experiment, NOE difference spectroscopy, or single-crystal X-ray crystallographic analysis. The absolute configurations of all stereoisomers were established by the CD spectra in conjunction with ECD calculations. Furthermore, the construction pathways of indolchromins A (**4**) and B (**5**) were elucidated by enzyme inhibition, precursor feeding experiments, and energy calculation. This study pinpointed that AONS could catalyse carbon–carbon bond formation in fungal culture *via* the decarboxylative Claisen condensation reaction through accepting indole and polyketide as substrates. In aggregation, this work characterizes indolchromins A (**4**) and B (**5**) as skeletally unprecedented indole alkaloids with promising antibacterial and cytotoxic activities, and provides a generalizable eco-friendly approach to the structurally undescribed polyketide-indole hybrids with promising biological properties.

4. Experimental

4.1. General experimental procedures

Optical rotations were recorded in MeOH on a Rudolph Research Analytical Autopol IV automatic polarimeter. IR spectra were acquired in KBr disks on a Nexus 870 FT–IR spectrometer. MS spectra were determined on an Agilent 6210 LC/TOF-MS spectrometer operating in a positive mode with direct infusion. NMR spectra were measured on a Bruker DRX400 or Varian Inova-600 NMR spectrometer with TMS as an internal standard. CD spectra were recorded on a JASCO J-810 Chirascan. HPLC separation was performed using Waters octadecylsilyl (ODS) column (250 mm × 10 mm, 5 μm), a Hitachi pump L-7100, and a UV detector L-7400. Silica gel (200–300 mesh) for column chromatography (CC) and GF$_{254}$ (10–20 mm) for thin layer chromatography (TLC) were produced by the Qingdao Marine Chemical Company, China. The ODS silica gel (50 μm) was purchased from YMC Co., Ltd., Japan, and Sephadex LH-20 from Pharmacia Biotech, Sweden. All drugs used herein as positive controls for bioassays were purchased from Sigma–Aldrich Co. Reagents and solvents used in the study were of analytical grade. Chiral HPLC separation was performed on a chiral column (CHIRALPAK® IA, Lot No. IA00CG-RE001, 250 mm × 10 mm) with *n*-hexane/ethanol mixtures for different stereoisomers (Supporting Information Table S1). The human/animal bacterial pathogens were obtained from the First Affiliated Hospital of Nanjing Medical University (Nanjing, China), and the plant pathogenic bacteria were obtained from Nanjing Agricultural University (Nanjing, China).

4.2. Fungal cultivation and extraction

D. eschscholzii was cultured on Petri dishes in potato dextrose agar (PDA) medium at 28 °C for 3 days. The fresh mycelia taken from the grown fungal colony was inoculated into the flasks (always one-liter sized), each containing 400 mL of malt extract (ME) medium (20 g/L malt extract, 20 g/L sucrose and 1 g/L peptone). After a 2-day incubation at 28 °C with an agitation (200 rpm , DZ-900 agitator , Taicang Qiang Le Experimental Equipment Co., Ltd.), 20 mL of culture liquid was transferred as inoculating seed into each flask containing 400 mL of ME medium. At 24, 48, and 72 h after inoculation, I3C (**1**) was added into the flasks up to its concentration at 1.0 mmol/L. Cultivations were continued for the ensuing 10 days at 28 °C with agitation (200 rpm). The whole culture was extracted with ethyl acetate (EtOAc).

4.3. Preparation of intracellular fungal proteins (IFPs)

As described in previous studies[6,36,37], the IFP was extracted at 4 °C from the fungal mycelia, which were collected by filtering with a Buchner funnel from the fungal culture. After washed twice with distilled water, frozen in liquid nitrogen, and ground into fine powder, the protein fraction was suspended in phosphate buffer saline (PBS, pH = 7.0 throughout, unless stated otherwise), ultra-sonicated for 30 min, and centrifuged at 11,486 × *g* for 20 min. The supernatant was collected with its protein concentration quantified by using the BCA (bicinchoninic acid) Protein Assay Kit.

4.4. ECD computational details

The DFT at B3LYP/6–31G (d,p) level was employed to optimize the geometries of the studied systems, taking crystal structures as the original configurations. The solvent effect on the electronic structures of the concerned systems were evaluated by the quantum chemistry method through the polarizable continuum model (PCM, dielectric constant ε = 32.64 for MeOH). The corresponding excited-state calculations were performed at the ground-state optimized geometries. Time-dependent DFT in combination with PCM model (TD-DFT/PCM) with the same basis set was carried out to calculate the spin-allowed excitation energy and rotatory strength of the lowest 100 excited states. The UV and ECD spectra were generated using the program SpecDis[38] by applying a Gaussian band shape with the width of 0.20 eV, from oscillator strengths and dipole-velocity rotational strengths, respectively.

4.5. Relative energy computational details

DFT at the B3LYP/6–31+G (d,p) level was applied to optimize the geometries of the studied systems. Based on the optimized conformations, the vibrational frequency calculations using B3LYP method with 6–31+G(d,p) basis were performed to all stationary points to check whether the optimized geometry corresponded to a minimum or transition state and to obtain the Gibbs free energies. The solvent effects on the energies were evaluated by PCM model (dielectric constant ε = 78.39 for H_2O). All the calculations were performed with the Gaussian 09 program[39].

4.6. Singlet crystal X-ray diffraction

Structures were solved by the direct method (SHELXS-97) and refined using full-matrix least-squares difference Fourier techniques. Crystallographic data in CIF format have been deposited in the Cambridge Crystallographic Data Centre [available free of charge at http://www.ccdc.cam.ac.uk/deposit or from the CCDC, 12 Union Road, Cambridge CB21EZ, UK; fax: (+44) 1223-336-033; or e-mail: deposit@ccdc.cam.ac.uk].

4.6.1. Crystal data for (+)-(2S,4R)-4/(−)-(2R,4S)-4 racemate

Performed at 293 K on an Agilent SuperNova diffractometer equipped with Mo–Kα radiation (λ = 0.71073 Å). $C_{18}H_{17}NO_2$, M_r = 279.33, monoclinic, space group P21/c, a = 9.951 (2) Å, b = 8.6200 (17) Å, c = 16.760 (3) Å, V = 1411.2 (5) Å, Z = 4, D_x = 1.315 g/cm^3, μ = 0.086 mm^{-1} and F (000) = 592.0; crystal dimensions: 0.30 × 0.20 × 0.10 mm^3; 1351 unique reflections with 2581 obeying the $I > 2\sigma$ (I) cutoff; R_1 = 0.0723, wR_2 = 0.2123, S = 1.005; Supporting Information publication No. CCDC-1483095.

4.6.2. Crystal data for (−)-(2S,4S)-4/(+)-(2R,4R)-4 racemate

Performed at 100 K on an Agilent SuperNova diffractometer equipped with Cu–Kα radiation (λ = 1.54178 Å). $C_{18}H_{17}NO_2$, M_r = 279.33, orthorhombic, space group P21 21 21, a = 9.2670 (6) Å, b = 10.6210 (6) Å, c = 29.8392 (18) Å, V = 2936.9 (3) Å, Z = 8, D_x = 1.263 g/cm^3, μ = 0.657 mm^{-1} and F (000) = 1184.0; crystal dimensions: 0.34 × 0.28 × 0.25 mm^3; 4386 unique reflections with 4882 obeying the $I > 2\sigma$ (I) cutoff; R_1 = 0.0275, wR_2 = 0.0802, S = 1.099; Supporting Information publication No. CCDC-1483093.

4.7. Isolation and identification of stereoisomers of 4 and 5

4.7.1. Fractionation

The EtOAc extract (83 g) derived from the fungal culture (Section 4.2) was separated into seven fractions over a silica gel column with petroleum ether/acetone mixtures (always *v/v*; 100:2, 100:5, 10:1, 5:1, 3:1, 2:1, and 1:1). LC–HR/MS analysis pinpointed an alkaloid-containing CC fraction which was separated *via* CC over ODS with a gradient of MeOH/H_2O (30:70→100:0) to give subfractions I and II. Subfraction I therefrom was subjected to Sephadex LH-20 with MeOH and purified further by semi-preparative HPLC with MeOH/H_2O (60:40) to give a racemate, which was separated into (+)-(2S,4R)-4 (12 mg, yield 0.01%) and (−)-(2R,4S)-4 (17 mg, yield 0.02%) by chiral HPLC (Supporting Information Table S1 and Fig. S1). The mother liquors yielded above were combined and purified to supply a crystal, which gave (−)-(2S,4S)-4 (6.5 mg) and (+)-(2R,4R)-4 (6 mg) by chiral HPLC (Supporting Information Table S1 and Fig. S1). Subfraction II was fractionated by semi-preparative HPLC with MeOH/H_2O (75:25) to give two racemates, which afforded (+)-(2S,4R)-5 (6 mg), (−)-(2R,4S)-5 (5.5 mg), (−)-(2S,4S)-5 (4 mg), and (+)-(2R,4R)-5 (3 mg) by chiral HPLC separation (Supporting Information Table S1 and Figs. S14−S15).

4.7.2. Physical constants and spectral data

4.7.2.1. (2S,4R)-4/(2R,4S)-4 racemate. Light yellow crystal from MeOH; IR (KBr) ν_{max} 3409, 2971, 2913, 1616, 1587, 1464, 744 cm^{-1}; ^{1}H and ^{13}C NMR data assigned in Table 1.

(+)-(2S,4R)-4. Light grey powder, HR-ESI-MS: *m/z* 302.1159; $[\alpha]_D^{25}$+25.3 (c = 0.15, MeOH), CD (MeOH) λ_{max} ($\Delta\varepsilon$) = 204 (5.5), 228 (−6.1) and 270 (1.38) nm.

(−)-(2R,4S)-4. Light grey powder, HR-ESI-MS: *m/z* 302.1154; $[\alpha]_D^{25}$ −20.0 (c = 0.10, MeOH), CD (MeOH) λ_{max} ($\Delta\varepsilon$) = 204 (−4.4), 228 (5.2) and 273 (−0.88) nm.

4.7.2.2. (2S,4S)-4/(2R,4R)-4 racemate. Light yellow crystal from MeOH; IR (KBr) ν_{max} 3421, 2960, 2924, 2854, 1617, 1464, 803 cm^{-1}; ^{1}H and ^{13}C NMR data assigned in Table 1.

(−)-(2S,4S)-4. Light yellow powder, HR-ESI-MS: *m/z* 302.1157; $[\alpha]_D^{25}$ −26.4 (c = 0.27, MeOH), CD (MeOH) λ_{max} ($\Delta\varepsilon$) = 207 (13.5), 230 (−7.7), and 277 (2.3) nm.

(+)-(2R,4R)-4. Light grey powder, HR-ESI-MS: *m/z* 302.1158; $[\alpha]_D^{25}$ +33.9 (c = 0.11, MeOH); CD (MeOH) λ_{max} ($\Delta\varepsilon$) = 207 (−17.9), 230 (10.41), and 277 (−2.67) nm.

4.7.2.3. (2S,4R)-5/(2R,4S)-5 racemate. Light brown powder; IR (KBr) ν_{max} 3409, 2927, 1617, 1461, 1384, 746 cm^{-1}; ^{1}H and ^{13}C NMR data assigned in Table 1.

(+)-(2*S*,4*R*)-**5**. Light brown powder, HR-ESI-MS: *m/z* 431.1731, $[\alpha]_D^{25}$ +20.0 (*c* = 0.10, MeOH), CD (MeOH) λ_{max} ($\Delta\varepsilon$) = 209 (−5.62), 236 (2.82), and 275 (−1.18) nm.

(−)-(2*R*,4*S*)-**5**. Light brown powder, HR-ESI-MS: *m/z* 431.1729, $[\alpha]_D^{25}$ −22.1 (*c* = 0.27, MeOH), CD (MeOH) λ_{max} ($\Delta\varepsilon$) = 204 (18.6), 239 (−2.51), and 279 (2.23) nm.

4.7.2.4.   (2S,4S)-5/(2R,4R)-5 racemate. Light brown powder; IR (KBr) ν_{max} 3408, 2927, 1617, 1230, 1100, 600 cm^{-1}; ^{1}H and ^{13}C NMR data assigned in Table 1.

(−)-(2*S*,4*S*)-**5**. Light brown powder, HR-ESI-MS: *m/z* 431.1732, $[\alpha]_D^{25}$ −40.0 (*c* = 0.12, MeOH), CD (MeOH) λ_{max} ($\Delta\varepsilon$) = 201 (−16.8), 239 (2.12), and 278 (−1.84) nm.

(+)-(2*R*,4*R*)-**5**. Light brown powder, HR-ESI-MS: *m/z* 431.1732, $[\alpha]_D^{25}$ +32.3 (*c* = 0.11, MeOH), CD (MeOH) λ_{max} ($\Delta\varepsilon$) = 209 (5.64), 236 (−2.87), and 275 (1.15) nm.

4.8.   Capture of 3-MEI

A drop of HCl (37%) was added to a solution of I3C (**1**, 100 mg, 0.68 mmol) in 7 mL of CH$_3$CN. After stirred for 30 min, 2-mercaptoethanol (0.15 mL, 2.04 mmol) was added and the reaction mixture was stirred at room temperature for 24 h. The reaction was quenched by adding saturated NaHCO$_3$ (10 mL) followed by extraction with CH$_2$Cl$_2$ (3 × 14 mL). The organic layer was washed with water and dried over Na$_2$SO$_4$. Removal of the solvent gave a residue which was purified by CC over silica gel with petroleum ether/ethyl acetate (10:1) to give the anticipated product 2-(3-indolylmethyl)thioethanol (101 mg, 72%), HR-ESI-MS: *m/z* 208.0797 [M+H]$^+$ (Calcd. for C$_{11}$H$_{13}$SNO, 208.0796), ^{1}H NMR (400 MHz, CDCl$_3$): δ_H 7.71 (d, *J* = 8.0 Hz, H-5), 7.38 (d, *J* = 8.0 Hz, H-8), 7.23 (t, *J* = 8.0 Hz, H-7), 7.15 (t, *J* = 8.0 Hz, H-6), 3.96 (s, H-3), 3.69 (t, *J* = 8.0 Hz, H-1), 2.69 (t, *J* = 8.0 Hz, H-2) (Supporting Information Fig. S32).

4.9.   Elucidation of transformation pathways

4.9.1.   Involvement of AONS in the production of 4 and 5
The fungus was cultured in the presence of **1** with exposure to each of AONS inhibitors D-cycloserine, plumbagin, and triphenyltin acetate (all at 1.0 mmol/L). The EtOAc extracts derived from these cultures were analyzed by LC–HR/MS. Co-supplementation of **1** with any of the three AONS inhibitors in the culture abolished the production of **4** and **5** (Fig. 5A). These findings collectively indicated that the fungal AONS catalyses the Claisen-condensation step towards these polyketide indoles (Fig. 5A).

4.9.2.   Non-enzymatic formation of 5 from 4 via incorporating 3-MEI
To the test tubes preloaded with IFPs (PBS as a blank control), **4** (0.2 mg) and **1** (0.38 mg) were added (Fig. 5B), followed by agitating for 24 h at 36 °C. The EtOAc extract derived from these treatments were analyzed by LC–HR/MS with the authentic samples co-assayed as controls. As a result, **5** could be produced by coupling of **4** with 3-MEI (derived from **1** *via* acidic dehydration) in the IFP-treated and -untreated (PBS) test tubes (Fig. 5B).

4.9.3.   Study the precursor of 4
To the test tubes preloaded with IFPs (PBS as a blank control), **1** (0.41 mg) and **3** (0.5 mg) or **1** (0.41 mg) and 5-hydroxy-2- methylchroman-4-one (0.5 mg) were added, followed by agitating for 24 h at 36 °C, respectively. The EtOAc extract derived from the treatment was analyzed by LC–HR/MS with the authentic samples co-assayed as control. Compound **4** was generated from **3**, but not from 5-hydroxy-2-methylchroman-4-one (Fig. 6A).

4.9.4.   Uninvolvement of 3,3′-diindolylmethane (DIM) in the generation of 5
To the test tubes preloaded with IFPs (PBS as a blank control), DIM (0.68 mg) and **3** (0.5 mg) were added, followed by agitating for 24 h at 36 °C. The EtOAc extract derived from the treatment was analyzed to be free of **5** by LC–HR/MS with the authentic samples co-assayed as control. Thus, **5** was not generated from DIM (Fig. 6B).

4.10.   Biological evaluations

4.10.1.   Antimicrobial assay
All stereoisomers of **4** and **5** were tested for the antimicrobial activity against the plant [*Erwinia amylovory* (Ea) and *Xanthomonas oryzae* pv. *oryzicola* (Xoo)] and human/animal pathogens [*C. perfringens* (Cp), *C. difficile* (Cd), *Veillonella* sp., *Bacteroides fragilis* (Bf), *Bacillus subtilis* (Bs), *Staphylococcus aureus* (Sa), and *Streptococcus pyogenes* (Sp)]. Broth microdilution was used to determine the minimum inhibitory concentrations (MICs) of samples. Duplicate 2-fold serial dilutions of the test sample (50 μL/well) were prepared in 96-well sterile polypropylene microtiter plates (LabServ, Fisher Scientific, China), in the appropriate broth containing 2% DMSO. A bacterial cell suspension (50 μL) corresponding to 1 × 10^6 CFU/mL was added in all wells except the wells reserved as blank (broth plus inoculum), negative (broth only) and positive controls (co-evaluated antibiotic). The final concentration of bacteria in the assay was 5 × 10^5 CFU/mL (or 5 × 10^4 CFU/well in the microdilution method), and that of DMSO was 1% (*v/v*). Incubate microtiter plates were then placed on a shaker for 10 min and incubated at 37 °C for 16–20 h or until satisfactory growth is obtained. After incubation, the MIC was determined as the lowest concentration at which no growth was observed in the duplicate wells. Streptomycin and tinidazole (Sigma–Aldrich, USA) were co-assayed as positive controls for the pathogenic bacteria and fungi, respectively. Antimicrobial assay was performed in triplicate[31,40], and the data are expressed as means ± SD (Table 2).

4.10.2.   Cytotoxicity assay
The cytotoxicity was evaluated on the eight human cancer cell lines (SW480, HL-60, HepG-2, A375, MCF-7, CaoV-3, A549, and MDA-MB-231) by MTT [3-(4,5-dimethyl-2-thiazolyl)-2,5-diphenyl-2-*H*-tetrazolium bromide] assay as described[41]. Briefly, the test cell at the exponential growth phase were collected and transferred into 96-well plates. After incubated for 24 h, sample dilutions were dispensed to the established culture plates. Two days (48 h) later, the MTT solution (0.1 mg per well) was then added to each well. After further incubation for 4 h, the supernatant was removed, the crystals were fully dissolved in DMSO (150 mL), and the absorbance of each well was read at 570 nmol/L (Sunrise, Tecan). The IC$_{50}$ value was determined as the concentration, at which a half of the test cell growth was inhibited. The experiment was performed in triplicate[42], and the data are expressed as means ± SD (Table 3).

Acknowledgments

Appendix A. Supporting information

Supplementary data associated with this article can be found in the online version at https://doi.org/10.1016/j.apsb.2018.09.011.

References

1. Meng L, Guo Q, Liu Y, Chen M, Li Y, Jiang J, et al. Indole alkaloid sulfonic acids from an aqueous extract of *Isatis indigotica* roots and their antiviral activity. *Acta Pharm Sin B* 2017;**7**:334–41.

2. Liu Y, Wang X, Chen M, Lin S, Li L, Shi J. Three pairs of alkaloid enantiomers from the root of *Isatis indigotica*. *Acta Pharm Sin B* 2016;**6**:141–7.

3. Xu W, Gavia DJ, Tang Y. Biosynthesis of fungal indole alkaloids. *Nat Prod Rep* 2014;**31**:1474–87.

4. Butler MS, Robertson AA, Cooper MA. Natural product and natural product derived drugs in clinical trials. *Nat Prod Rep* 2014;**31**:1612–1661.

5. Mishra BB, Tiwari VK. Natural products: an evolving role in future drug discovery. *Eur J Med Chem* 2011;**46**:4769–807.

6. Lin LP, Yuan P, Jiang N, Mei YN, Zhang WJ, Tan RX, et al. Gene-inspired mycosynthesis of skeletally new indole alkaloids. *Org Lett* 2015;**17**:2610–3.

7. Xu J, Lacoske MH, Theodorakis EA. Neurotrophic natural products: chemistry and biology. *Angew Chem Int Ed* 2014;**53**:956–87.

8. Lyssiotis CA, Lairson LL, Boitano AE, Wurdak H, Zhu ST, Schultz PG. Chemical control of stem cell fate and developmental potential. *Angew Chem Int Ed* 2011;**50**:200–41.

9. Pan Z, Qin XJ, Liu YP, Wu T, Luo XD, Xia C. Alstoscholarisines H–J, indole alkaloids from *Alstonia scholaris*: structural evaluation and bioinspired synthesis of alstoscholarisine H. *Org Lett* 2016;**18**:654–7.

10. Leng L, Zhou X, Liao Q, Wang F, Song H, Zhang D, et al. Asymmetric total syntheses of Kopsia indole alkaloids. *Angew Chem Int Ed* 2017;**56**:3703–7.

11. Chen W, Yang XD, Tan WY, Zhang XY, Liao XL, Zhang H. Total synthesis of (–)-vindorosine. *Angew Chem Int Ed* 2017;**56**:12327–31.

12. Zhang Q, Pang B, Ding W, Liu W. Aromatic polyketides produced by bacterial iterative type I polyketide synthases. *ACS Catal* 2013;**3**:1439–1447.

13. Liang X, Zhang TY, Zeng XY, Zheng Y, Wei K, Yang YR. Ir-catalyzed asymmetric total synthesis of (–)-Communesin F. *J Am Chem Soc* 2017;**139**:3364–7.

14. Li Y, Zhang Q, Du Q, Zhai H. Rh-catalyzed [3+2] cycloaddition of 1-sulfonyl-1,2,3-triazoles: access to the framework of aspidosperma and kopsia indole alkaloids. *Org Lett* 2016;**18**:4076–9.

15. Tang XD, Wu WQ, Zeng W, Jiang HF. Copper-catalyzed oxidative carbon–carbon and/or carbon–heteroatom bond formation with O_2 or internal oxidants. *Acc Chem Res* 2018;**51**:1092–105.

16. Bietti M. Activation and deactivation strategies promoted by medium effects for selective aliphatic C3H bond functionalization. *Angew Chem Int. Ed.* 2018 http://dx.doi.org/10.1002/anie.201804929.

17. Wang X, Lerchen A, Gensch T, Knecht T, Daniliuc CG, Glorius F. Combination of Cp*Rh^{III}-catalyzed C-H activation and a Wagner-Meerwein-type rearrangement. *Angew Chem Int Ed* 2017;**56**:1381–4.

18. Adwas AA, Elkhoely AA, Kabel AM, Abdel-Rahman MN, Eissa AA. Anti-cancer and cardioprotective effects of indol-3-carbinol in doxorubicin-treated mice. *J Infect Chemother* 2016;**22**:36–43.

19. Palani K, Harbaum-Piayda B, Meske D, Keppler JK, Bockelmann W, Heller KJ, et al. Influence of fermentation on glucosinolates and glucobrassicin degradation products in sauerkraut. *Food Chem* 2016;**190**:755–62.

20. Ciska E, Drabińska N, Honke J, Narwojsz A. Boiled Brussels sprouts: a rich source of glucosinolates and the corresponding nitriles. *J Funct Foods* 2015;**19**:91–9.

21. Anderton MJ, Manson MM, Verschoyle RD, Gescher A, Lamb JH, Farmer PB, et al. Pharmacokinetics and tissue disposition of indole-3-carbinol and its acid condensation products after oral administration to mice. *Clin Cancer Res* 2004;**10**:5233–41.

22. Hertweck C. The biosynthetic logic of polyketide diversity. *Angew Chem Int Ed* 2010;**48**:4688–716.

23. Zhang YL, Zhang J, Jiang N, Lu YH, Wang L, Tan RX, et al. Immunosuppressive polyketides from mantis-associated *Daldinia eschscholzii*. *J Am Chem Soc* 2011;**133**:5931–40.

24. Weems JM, Yost GS. 3-Methylindole metabolites induce lung CYP1A1 and CYP2F1 enzymes by AhR and non-AhR mechanisms, respectively. *Chem Res Toxicol* 2010;**23**:696–704.

25. Dai JQ, Krohn K, Draeger S, Schulz B. New naphthalene-chroman coupling products from the endophytic fungus, *Nodulisporium* sp. from *Erica arborea*. *Eur J Org Chem* 2009;**10**:1564–9.

26. Alvarez-Cisneros C, Muñoz MA, Suárez-Castillo OR, Pérez-Hernández N, Cerda-García-Rojas CM, Morales-Ríos MS, et al. Stereospecific $^5J_{\text{Hortho,OMe}}$ couplings in methoxyindoles, methoxycoumarins, and methoxyflavones. *Magn Reson Chem* 2014;**52**:491–9.

27. Kakita VM, Hosur RV. Hadamard homonuclear broadband decoupled TOCSY NMR: improved efficacy in detecting long-range chemical shift correlations. *Chemphyschem* 2016;**17**:4037–42.

28. Fridkin SK, Hageman JC, Morrison M, Sanza LT, Como-Sabetti K, Jernigan JA, et al. Methicillin-resistant *Staphylococcus aureus* disease in three communities. *Engl J Med* 2005;**352**:1436–44.

29. Esposito S, Bianchini S, Fastiggi M, Fumagalli M, Andreozzi L, Rigante D. Geoepidemiological hints about *Streptococcus pyogenes* strains in relationship with acute rheumatic fever. *Autoimmun Rev* 2015;**14**:616–21.

30. Aćimović SG, Zeng Q, McGhee GC, Sundin GW, Wise JC. Control of fire blight (*Erwinia amylovora*) on apple trees with trunk-injected plant resistance inducers and antibiotics and assessment of induction of pathogenesis-related protein genes. *Front Plant Sci* 2015;**6**:16.

31. Wiegand I, Hilpert K, Hancock RE. Agar and broth dilution methods to determine the minimal inhibitory concentration (MIC) of antimicrobial substances. *Nat Protoc* 2008;**3**:163–75.

32. Clocchiatti A, Cora E, Zhang Y, Dotto GP. Sexual dimorphism in cancer. *Nat Rev Cancer* 2016;**16**:330–9.

33. Han WB, Lu YH, Zhang AH, Zhang GF, Mei YN, Tan RX, et al. Curvulamine, a new antibacterial alkaloid incorporating two undescribed units from a *Curvularia* species. *Org Lett* 2014;**16**:5366–5369.

34. Hwang IT, Choi JS, Song HY, Cho SJ, Lim HK, Park NJ, et al. Validation of 7-keto-8-aminopelargonic acid synthase as a potential herbicide target with lead compound triphenyltin acetate. *Pestic Biochem Phys* 2010;**97**:24–31.

35. Asai T, Tsukada K, Ise S, Shirata N, Hashimoto M, Fujii I, et al. Use of a biosynthetic intermediate to explore the chemical diversity of pseudo-natural fungal polyketides. *Nat Chem* 2015;**7**:737–43.

36. Song YN, Jiao RH, Zhang WJ, Zhao GY, Dou H, Jiang R, et al. New ansamycin derivatives generated by simultaneous mutasynthesis. *Org Lett* 2015;**17**:556–9.

37. Yan W, Ge HM, Wang G, Jiang N, Mei YN, Jiang R, et al. Pictet-Spengler reaction-based biosynthetic machinery in fungi. *Proc Natl Acad Sci U S A* 2014;**111**:18138–43.

38. Bruhn T, Schaumlöffel A, Hemberger Y, Bringmann G. SpecDis: quantifying the comparison of calculated and experimental electronic circular dichroism spectra. *Chirality* 2013;**25**:243–9.

39. Frisch MJ, Trucks GW, Schlegel HB, Scuseria GE, Robb MA, Cheeseman JR, et al. *Gaussian 09, Revision D.01*. Wallingford, CT: Gaussian, Inc; 2013.

40. Périllaud C, Pilmis B, Diep J, Péan de Ponfilly G, Vidal B, Couzigou C. Prospective evaluation of rapid antimicrobial susceptibility testing by disk diffusion on Mueller-Hinton rapid-SIR directly on blood cultures. *Diagn Microbiol Infect Dis* 2018 pii: S0732-8893(18)30252-9.

41. Menicagli R, Samaritani S, Signore G, Vaglini F, Dalla Via L. *In vitro* cytotoxic activities of 2-alkyl-4,6-diheteroalkyl-1,3,5-triazines: new molecules in anticancer research. *J Med Chem* 2004;**47**: 4649–52.

42. Ge HM, Yu ZG, Zhang J, Wu JH, Tan RX. Bioactive alkaloids from endophytic *Aspergillus fumigatus*. *J Nat Prod* 2009;**72**:753–5.